Chemical Physics Letters 583 (2013) 119–124

Contents lists available at ScienceDirect

Chemical Physics Letters

journal homepage: www.elsevier.com/locate/cplett

Reactivity of adducts relevant to the deposition of hexagonal BN from first-principles calculations

R.R.Q. Freitas [a,b], G.K. Gueorguiev [b,*], F. de Brito Mota [a], C.M.C. de Castilho [a,c], S. Stafström [b], A. Kakanakova-Georgieva [b]

[a] Grupo de Física de Superfícies e Materiais, Instituto de Física, Universidade Federal da Bahia, Campus Universitário da Federação, 40170-115 Salvador, Bahia, Brazil
[b] Department of Physics, Chemistry and Biology (IFM), Linköping University, 581 83 Linköping, Sweden
[c] Instituto Nacional de Ciência e Tecnologia em Energia e Ambiente (CIENAM) INCT-E&A, Universidade Federal da Bahia, Salvador, Bahia, Brazil

ARTICLE INFO

Article history:
Received 22 March 2013
In final form 30 July 2013
Available online 6 August 2013

ABSTRACT

First-principles calculations, which also implement the nudged elastic band (NEB) code, are performed to investigate (i) the stability of the $(C_2H_5)_3B{:}NH_3$ adduct formed by the initial precursor molecules triethylborane $(C_2H_5)_3B$ and ammonia NH_3 in the metal–chemical-vapor-deposition (MOCVD) of hexagonal BN, and (ii) the energy barrier to the first ethane elimination through consistent unimolecular, ammonia-assisted, and adduct-assisted reaction pathways. Comparison is done with the reference case of the $(CH_3)_3Al{:}NH_3$ adduct, notoriously known for its high degree of stability and reactivity, which determines an overall severe parasitic gas-phase chemical reaction mechanism in the deposition of AlN.

1. Introduction

Aluminum nitride (AlN) and high-Al-content AlGaN alloys are reputed as the technologically relevant wide-band-gap semiconductor material system for the development of deep ultraviolet (UV), $\lambda < 280$ nm, light emitting diodes (LEDs) [1,2]. Hexagonal boron nitride (BN) has also made appearance as a material of direct wide-band-gap properties giving rise to intense room-temperature deep UV emission and even lasing at 215 nm in electron excitation experiments [3]. Most importantly, the achievement of hexagonal BN layers has been approached by the metal–organic-chemical-vapor-deposition (MOCVD), and on typical – considering the AlN-based deep UV LEDs – substrates such as SiC [4] and sapphire [5,6]. Previous explorative research into the MOCVD of BN-related materials and their properties is done targeting either the achievement of single phase AlBN solid solutions for lattice matching in the AlGaN/SiC system [7] or high-quality quaternary BAlGaN lattice matched to AlN and BAlGaN/AlN multiple quantum well structures for deep UV emission [8]. Very recent advances are reported on the MOCVD of p-type Mg-doped hexagonal BN on sapphire substrates [9] and on n-type Si-doped AlGaN templates [10], which suggests hexagonal BN/AlGaN p–n junction as an alternative device structure for deep UV photonics.

A successful MOCVD of high quality crystalline hexagonal BN layers requires high process temperatures, ~1300 °C [9,11], considering the strong B–N bond and the need for adequate surface diffusion. Typical precursors are triethylborane, $(C_2H_5)_3B$, and ammonia, NH_3, referred as to participate in parasitic gas-phase chemical reactions [5,11,12], which may essentially be activated by the high process temperatures.

The development of severe parasitic gas-phase chemical reactions in the reference case of the MOCVD of AlN – which implements typical precursors such as trimethylaluminum, $(CH_3)_3Al$, and NH_3 at high process temperatures (>1100 °C) [13] – is considered in connection to the high degree of reactivity of the $(CH_3)_3Al{:}NH_3$ adduct. This adduct is formed instantaneously upon mixing of the precursors, and already at room temperature. The NH_3 precursor molecule readily donates electron-lone pair to the electron-deficient $(CH_3)_3Al$ precursor, the central metal atom of which has an empty p-orbital [14]. The formation of the $(CH_3)_3Al{:}NH_3$ adducts triggers intricate gas-phase chemistry dominated by the propagation of high-order oligomers $[(CH_3)_2AlNH_2]_n$, $n \geqslant 3$, following the easy dimerization of the amide monomer $(CH_3)_2AlNH_2$ [15]. The intricate gas-phase chemistry underlying the MOCVD of AlN is thoroughly debated [15–20] due to its impact on the operation of efficient, reproducible and controllable deposition process.

A variety of group-III R_3M and group-V YH_3 precursors, M = Al, Ga, In; R = CH_3, C_2H_5; and Y = N, P, As, is implemented in the MOCVD of a whole class of III–V semiconductor materials such as AlGaInAsP and more recently AlGaInN [20]. These precursors share the same coordination characteristics as $(CH_3)_3Al$ and NH_3. Experimental and theoretical investigations of the initial formation and subsequent reactivity of adducts formed by the respective

* Corresponding author.
E-mail address: gekos@ifm.liu.se (G.K. Gueorguiev).

0009-2614/$ - see front matter © 2013 Elsevier B.V. All rights reserved.
http://dx.doi.org/10.1016/j.cplett.2013.07.077

group-III and -V precursors have been of key importance to advance the understanding and optimization of MOCVD processes relevant to the achievement of device-quality semiconductor structures.

The importance of the adducts $R_3M{:}YH_3$, M = Al, Ga, In; R = CH_3, C_2H_5; and Y = N, P, As, which form between group-III R_3M and group-V YH_3 precursors under the conditions of the MOCVD of a variety of III–V semiconductors, is known to depend on the relative magnitude of their stability and the energy barrier to RH (i.e., n-alkanes, including methane, CH_4, alternatively, ethane, C_2H_6) elimination [14]. The gas-phase chemistry involved in the MOCVD of BN has not been addressed yet. We note though the implementation of a certain growth approach – the flow-rate modulation epitaxy – motivated to alleviate the anticipated parasitic side of gas-phase chemical reactions in the MOCVD of BN [11].

The present study is focused on achieving a better comprehension of essential aspects of the MOCVD chemistry of BN by performing first-principles calculations of the stability of the $(C_2H_5)_3B{:}NH_3$ adduct and the energy barrier to the first ethane elimination. This can determine the reactivity of the $(C_2H_5)_3B{:}NH_3$ adduct in the gas-phase and its potential to undergo evolution towards adduct-derived species which may be of relevance for the actual deposition mechanism underlying the MOCVD of BN.

2. Methodology rationale and computational details

The modeling of reaction species, which represent corresponding initial reactants, transition states (TSs) and final adduct-derived products, is performed within the framework of the density functional theory (DFT). The equilibrium structures of all species are depicted in Figure 1, and their bond lengths are listed in Table 1. At the first stage of the simulation procedure, the equilibrium structures of all reaction species are optimized by employing the Perdew–Wang exchange–correlation functional (PW91) [21] within the generalized gradient approximation (GGA) to DFT, as implemented in the Gaussian 03 code [22]. The PW91 exchange–correlation functional has been used before as a well performing alternative method to the Becke 3-parameter exchange Lee–Yang–Parr correlation hybrid functional (B3LYP) to simulate the structures of reaction species relevant to the MOCVD of AlGaInN [19]. In a more general context, the PW91 exchange–correlation functional may be preferred when the chemistry of n-alkanes (e.g., methane, ethane) is involved [23]. The 6-31G* basis set is employed for all atoms. At the next stage of the simulation procedure, the optimized structures of reaction species are employed for modeling reaction pathways. The VASP code [24] at the PW91 level of theory is adopted, making use of the projector augmented wave (PAW) method [25] and a plane wave basis set. The plane wave basis is expanded up to a cut-off energy of 800 eV. A single Γ-point is adopted as k-point sampling.

The nudged elastic band (NEB) code within the VASP package [26–28] – a very adequate, modern, and powerful numerical tool – is chosen to determine the minimum energy paths (MEPs) and transition states, for which a sequence of discrete 'images' is produced. Each 'image' corresponds to a specific geometry of the atoms on their way from a fixed initial to a fixed final state. Standard NEB [26] calculations are performed for approximately 100 ionic steps to achieve an approximate convergence for a specific MEP. In order to obtain a rigorous convergence to a transition state associated to this specific MEP, the standard NEB calculations are followed by applying the climbing-image NEB algorithm (CI-NEB) [29], so that the 'image' reaches the exact saddle point. In all energy barrier calculations performed, the number of 'images' (including the initial and final 'images') is set to ten which is important because of the correlation between a higher number of

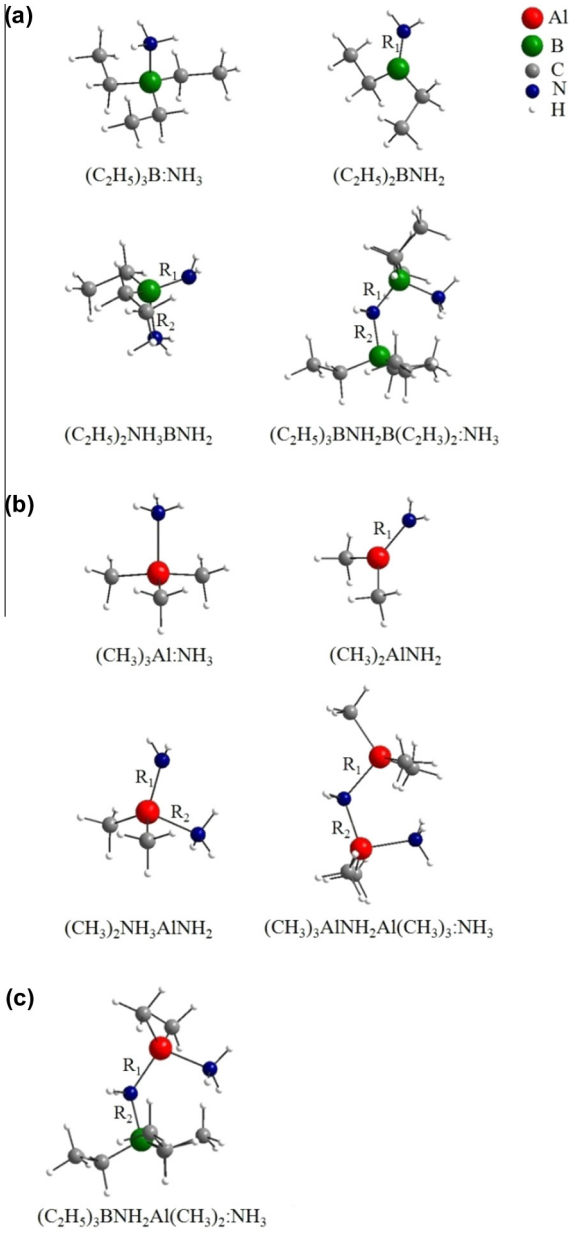

Figure 1. Equilibrium structures of reaction species relevant to the investigated gas-phase reaction pathways of: (a) ethane elimination in the $(C_2H_5)_3B + NH_3$ system; (b) methane elimination in the $(CH_3)_3Al + NH_3$ system; (c) methane elimination in the mixed $(C_2H_5)_3B + (CH_3)_3Al + NH_3$ system.

Table 1
Bond lengths R_1 (Å) and R_2 (Å), as indicated in Figure 1, of the equilibrium structures of reaction species relevant to investigated gas-phase reaction pathways of ethane/methane elimination in the $(C_2H_5)_3B + NH_3/(CH_3)_3Al + NH_3$ reactant systems.

Reaction species	R_1 (Å)	R_2 (Å)
$(C_2H_5)_2B{:}NH_3$	–	–
$(C_2H_5)_2BNH_2$	1.40	–
$(C_2H_5)_2NH_3BNH_2$	1.50	1.74
$(C_2H_5)_3BNH_2B(C_2H_5)_2{:}NH_3$	1.69	1.60
$(CH_3)_3Al{:}NH_3$	–	–
$(CH_3)_2AlNH_2$	1.78	–
$(CH_3)_2NH_3AlNH_2$	1.83	2.10
$(CH_3)_3AlNH_2Al(CH_3)_2{:}NH_3$	2.03	1.93
$(C_2H_5)_3BNH_2Al(CH_3)_2{:}NH_3$	1.94	1.68

'images' employed in a NEB calculation and an improved precision of a MEP determination. The NEB code is applied successfully to a wide range of problems with some of the most recent examples found elsewhere [30,31]. For the structural relaxations of the species involved, their constituent atoms are allowed to relax until the forces acting on each atom decrease below the value of 0.01 eV/Å. The total energy convergence criterion in both, geometry optimizations and electronic structure calculations, is set to be 10^{-5} eV.

3. Results and discussion

The instantaneous formation of the $(C_2H_5)_3B{:}NH_3$ adduct is considered as following the reaction:

$$(C_2H_5)_3B + NH_3 \leftrightarrow (C_2H_5)_3B : NH_3, \quad (1)$$

and in the context of the general framework of the formation – without any energy barrier – of adducts of the type $R_3M{:}YH_3$ between group-III R_3M and group-V YH_3 precursors, M = B, Al, Ga, In; R = H, CH_3, C_2H_5; and Y = N, P, As, [20]. The donor–acceptor bonding between the electron-rich group-V and the electron-deficient group-III precursors has been a subject of fundamental studies, particularly on the example of the ammonia borane adducts $H_3B{:}NH_3$ [20]. We point to the extensive DFT-based studies on the reactivity of different $(CH_3)_3M{:}NH_3$ adducts, M = Al, Ga, In, which is substantially dependent on the metal atom involved [15–20]. $(CH_3)_3Al$, respectively $(CH_3)_3Ga$, and $(CH_3)_3In$, is the typical group-III precursor in the MOCVD of AlN, GaN, and InN, and the deposition process has significantly been optimized. Alternative precursor, although less implemented, could be triethylaluminum, $(C_2H_5)_3Al$, respectively $(C_2H_5)_3Ga$, and $(C_2H_5)_3In$. Accordingly, few DFT-based studies treat the initial reactivity of the $(C_2H_5)_3M{:}NH_3$ adducts, M = Al, Ga, In [32]. There is no previous treatment of the reactivity of adducts relevant to the MOCVD of BN. We note that a successful precursor combination in the MOCVD of BN involves the group-III precursor triethylborane, $(C_2H_5)_3B$ [4–12]. Among the complex considerations in the choice of any precursor, the preference to $(C_2H_5)_3B$ – as may be compared to another potential precursor available in a liquid form, tributylborane [33] – is due to its volatility. The vapor pressure of $(C_2H_5)_3B$ is ~12.5 torr at 0 °C [34], which is appropriate in MOCVD conditions.

The $(C_2H_5)_3B$ precursor, like any other group-III ethyl, propyl, butyl alkyls, is expected to undergo unimolecular decomposition through β-elimination reaction. This may have consequences for the overall growth chemistry underlying the MOCVD process, and the material properties of the epitaxial layers. In the classical case study of the MOCVD of GaAs, decomposition reactions of group-III alkyls– active at or near the growing surface – contribute a basis for qualitative description of the growth trends in respect to the use of $(CH_3)_3Ga$, alternatively, $(C_2H_5)_3Ga$ precursors [35]. Particularly, the difference in the carbon incorporation into GaAs is explained with the difference in the reaction products from the decomposition of the corresponding precursors. The $(C_2H_5)_3Ga$ decomposition through β-elimination reaction with the formation of C_2H_4 is considered the important reaction pathway in the $(C_2H_5)_3Ga$-based MOCVD of GaAs. Ethyl radicals (which can take a hydrogen atom from AsH_3 to form C_2H_6), and $(C_2H_5)_3Ga{:}AsH_3$ adducts – which can also participate in the C_2H_6 elimination reaction [35] – are intermediate reaction products in this case [36]. Unlike the $(C_2H_5)_3Ga{:}AsH_3$ adduct, the $(C_2H_5)_3In{:}PH_3$ adduct in the $(C_2H_5)_3In$-based MOCVD of InP is strong enough and propagates the gas-phase with ethane elimination due to the reactivity of the hydrogen attached to the outer C (β-carbon) [36].

For the decomposition of individual precursors to be important under MOCVD conditions – and considered to directly reflect the operation of reactions at or near the growing surface [35] – the corresponding adduct needs to be unstable, which obviously applies to the case of GaAs. It is presented that the dissociation energy of the $R_3M{:}YH_3$ adducts, M = Al, Ga, In; R = CH_3, C_2H_5; Y = N, P, As, decreases in the order N ≫ P > As, and the stability of adducts decreases in the order Al > In ⩾ Ga [20]. The adducts between the group-III R_3M precursors and $NH_3$are essentially strong and can be dominating the MOCVD chemistry of III-Nitrides. Particularly, the $(CH_3)_3Al{:}NH_3$ adduct is notoriously known for its stability and subsequent facile methane elimination to form high-order oligomers [15], which certainly reflects the tendency of retention of the very strong Al–N coordination interaction [20].

Following the perceived instantaneous $(C_2H_5)_3B{:}NH_3$ adduct formation upon mixing of the precursors – and in the context of the considered general framework – ethane elimination is further considered consistent with the reaction pathways (2–4):

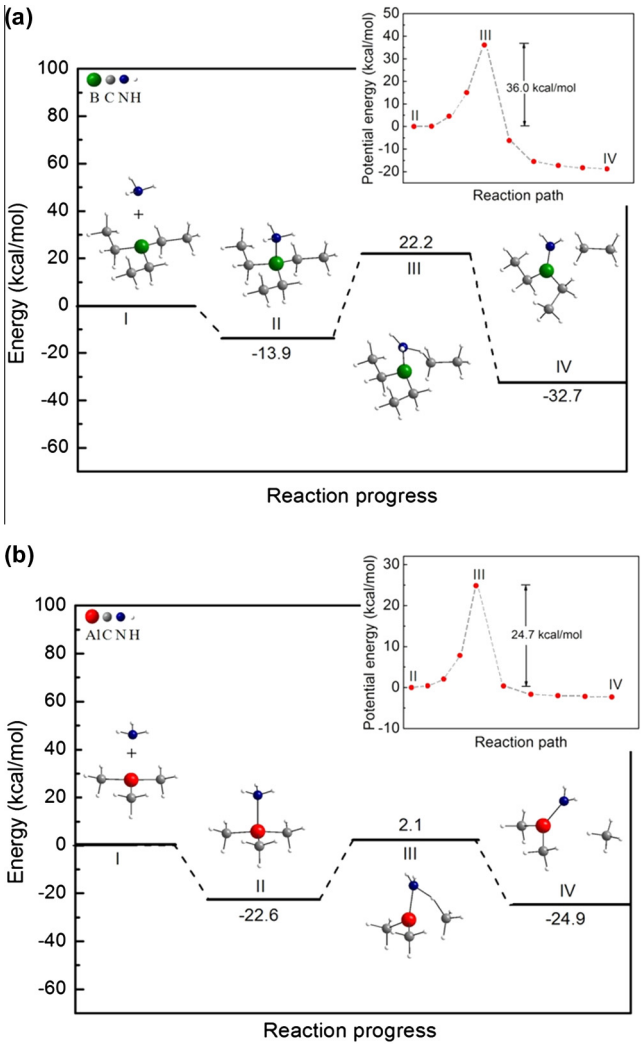

Figure 2. Schematic diagrams of sequences of gas-phase reactions starting with the formation of the (a) $(C_2H_5)_3B{:}NH_3$ adduct from the initial $(C_2H_5)_3B$ and NH_3 precursor molecules and further C_2H_6 elimination through the unimolecular reaction pathway (2); (b) $(CH_3)_3Al{:}NH_3$ adduct formation from the initial $(CH_3)_3Al$ and NH_3 precursor molecules and further CH_4 elimination through the unimolecular reaction pathway (5). The inset represents the minimum energy path between two equilibrium structures (II and IV) of the overall gas-phase reaction. The line drawn to connect the points serves the only purpose of guiding the eye. The equilibrium structures of reaction species, corresponding to sequential steps I-to-IV are depicted in each of the schematic diagrams.

$$(C_2H_5)_3B : NH_3 \rightarrow TS(2) \rightarrow (C_2H_5)_2BNH_2 + C_2H_6 \quad (2)$$

$$(C_2H_5)_3B : NH_3 + NH_3 \rightarrow TS(3) \rightarrow (C_2H_5)_2BNH_2 : NH_3 + C_2H_6 \quad (3)$$

$$(C_2H_5)_3B : NH_3 + (C_2H_5)_3B : NH_3 \rightarrow TS(4) \rightarrow (C_2H_5)_3BNH_2B(C_2H_5)_2 : NH_3 + C_2H_6 \quad (4)$$

where TS(2–4) stands for transition state.

Since ammonia is typically introduced in the gas-phase in the ratio of $NH_3/(C_2H_5)_3B$ ~210–2100 in the MOCVD of BN [5], the reaction pathway (3) can easily be assisted via collisions between the $(C_2H_5)_3B$:NH_3 adducts and the excess NH_3 molecules present in the gas-phase. High gas-flow rates of NH_3 and high process temperatures, typical in the MOCVD of BN (and AlN), imply that there is an excess of active N-bearing species readily available for deposition at the surface [15].

The C_2H_6 elimination following any of the unimolecular (2), ammonia-assisted (3) and adduct-assisted (4) reaction pathways essentially generates adduct-derived species, which can potentially evolve further by next steps of C_2H_6 elimination. Our purpose is, however, to evaluate the importance of the $(C_2H_5)_3B$:NH_3 adduct in the MOCVD of BN, which depends on the relative magnitude of its stability and the energy barrier to the first ethane elimination [14].

Figures 2a, 3a, and 4a represents schematic diagrams of sequences of gas-phase reactions starting with the formation of the $(C_2H_5)_3B$:NH_3 adduct from the initial $(C_2H_5)_3B$ and NH_3 precursor molecules. The adducts may eliminate ethane through the transition states TS(2–4) and evolve towards the adduct-derived species $(C_2H_5)_2BNH_2$, $(C_2H_5)_2BNH_2$:NH_3, and $(C_2H_5)_3BNH_2B(C_2H_5)_2$:$NH_3$, respectively. The equilibrium structures of all reaction species, as obtained following the described computational procedure, are depicted alongside with the corresponding sequential steps I-to-IV(V) in each of the schematic diagrams. Particularly, the geometry optimization of a transition state structure (i.e., a metastable structure), is a very demanding task [14], which has been solved by implementing adequate tools: the NEB and the CI-NEB codes. Energy barrier calculations (respective insets in Figures 2a, 3a, and 4a) allow relative energies of reaction species to be obtained with respect to the initial reactant system $(C_2H_5)_3B + NH_3$. The initial reactants and final configurations correspond to the reaction species associated with steps in each of the schematic diagrams in Figures 2a, 3a, and 4a, II to IV in the first case and III to V in the other two, respectively.

The discussion of the stability of the $(C_2H_5)_3B$:NH_3 adduct, and the energy barrier to the first RH (in this case C_2H_6) elimination through the reaction pathways (2–4), involves comparison with the stability of the reference $(CH_3)_3Al$:NH_3 adduct and the energy barrier to the first RH (in this case CH_4) elimination through the equivalent reaction pathways (5–7):

$$(CH_3)_3Al : NH_3 \rightarrow TS(5) \rightarrow (CH_3)_2AlNH_2 + CH_4 \quad (5)$$

$$(CH_3)_3Al : NH_3 + NH_3 \rightarrow TS(6) \rightarrow (CH_3)_2AlNH_2 : NH_3 + CH_4 \quad (6)$$

$$(CH_3)_3Al : NH_3 + (CH_3)_3Al : NH_3 \rightarrow TS(7) \rightarrow (CH_3)_3AlNH_2Al(CH_3)_2 : NH_3 + CH_4 \quad (7)$$

where TS(5–7) stands for transition state.

The equilibrium structures of the corresponding reaction species, as obtained after geometry relaxation, and the associated relative energies, as calculated with respect to the initial reactant system $(CH_3)_3Al + NH_3$, are depicted alongside with the sequential steps I-to-IV(V) in each of the schematic diagrams in Figures 2b, 3b, and 4b, respectively. The same simulation procedure, as in the case of the $(C_2H_5)_3B + NH_3$ reactant system, has been carried out.

The $(C_2H_5)_3B$ precursor molecule forms a stable adduct with ammonia expressed by the gain of energy of 13.9 kcal/mol (Figure 2a). On the other hand, the $(C_2H_5)_3B$:NH_3 adduct appears as considerably less stable than the reference $(CH_3)_3Al$:NH_3 adduct, which formation is exothermic by 22.6 kcal/mol (Figure 2b). This value compares well with previously published reaction energies for the $(CH_3)_3Al + NH_3$ system, i.e., an energy gain of 27.0 kcal/mol for the formation of the $(CH_3)_3Al$:NH_3 adduct and energy barrier to the first methane elimination of 26.0 kcal/mol [18]. The energy barrier to the first methane elimination through the transition state TS(5) has the value of 24.7 kcal/molin our calculations (Figure 2b). It determines a relative energy of TS(5) of only 2.1 kcal/mol with respect to the initial reactant system $(CH_3)_3Al + NH_3$ (Figure 2b). A larger energy barrier, 36.0 kcal/mol, to the first ethane elimination through the unimolecular reaction pathway (2) is calculated for the $(C_2H_5)_3B + NH_3$ system (Figure 2a).

It might be expected [18] that the joint impact of the following two aspects: (i) the relatively lower stability of the $(C_2H_5)_3B$:NH_3 adduct (as compared to the $(CH_3)_3Al$:NH_3 adduct), which is a factor for reversible relaxation to the initial precursor molecules (reaction (1)); and (ii) the larger energy barrier to the first ethane elimination, and the associated large relative energy of the corresponding transition state TS(2) as obtained with respect to the initial

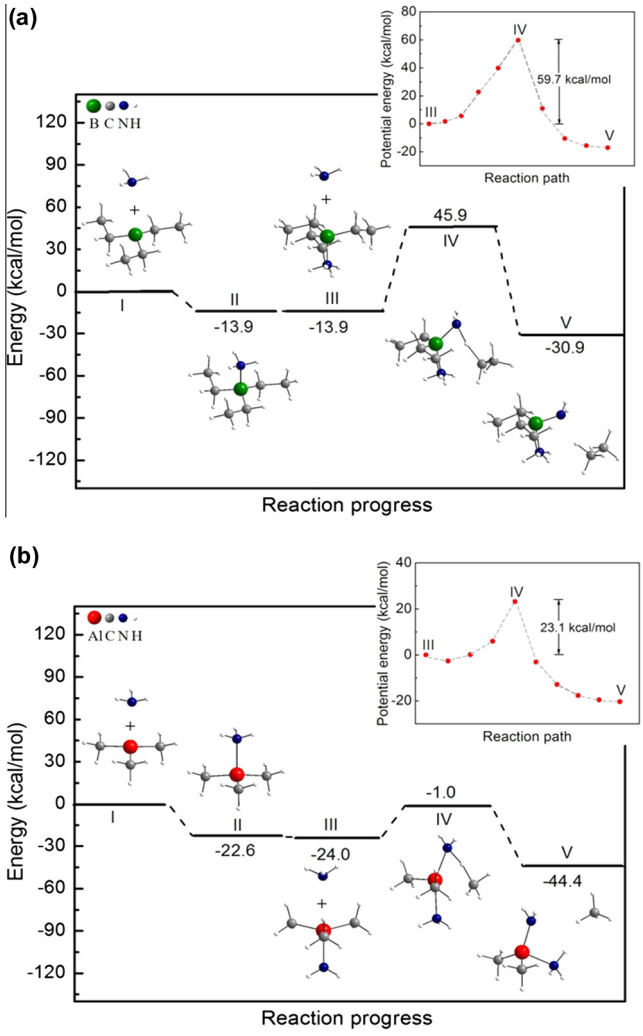

Figure 3. Schematic diagrams of sequences of gas-phase reactions starting with the formation of the (a) $(C_2H_5)_3B$:NH_3 adduct from the initial $(C_2H_5)_3B$ and NH_3 precursor molecules and further C_2H_6 elimination through the ammonia-assisted reaction pathway (3); (b) $(CH_3)_3Al$:NH_3 adduct formation from the initial $(CH_3)_3Al$ and NH_3 precursor molecules and further CH_4 elimination through the ammonia-assisted reaction pathway (6). The inset represents the minimum energy path between two equilibrium structures (III and V) of the overall gas-phase reaction. The line drawn to connect the points serves the only purpose of guiding the eye. The equilibrium structures of reaction species, corresponding to sequential steps I-to-V are depicted in each of the schematic diagrams.

reactant system $(C_2H_5)_3B + NH_3$ (Figure 2a);can preclude the reactivity of the $(C_2H_5)_3B{:}NH_3$ adduct in the gas-phase and its potential to undergo evolution towards adduct-derived species. The operation of the parasitic side of the gas-phase chemical reactions in the MOCVD of BN may not essentially be initiated. In this case, the decomposition of the initial precursors, $(C_2H_5)_3B$ and NH_3, and particularly at or near the growing surface, may dominate the actual deposition process of BN.

Possibility for crossing the energy barrier to the RH (R = CH_3, C_2H_5) elimination through corresponding transition states cannot be totally disregarded. It may successfully occur on the account of the quantized vibrational energy stored upon formation of the adducts, which are not in their ground states [37]. Further, adducts, and particularly excited adducts, are expected to climb the energy barrier to transition states, if adducts formation takes place under the conditions of high temperatures [17]. This is of particular concern in the MOCVD of BN, similarly to AlN, as it implies high process temperatures (~1300 °C). The above qualitative comments give reflection on the fact that the severity to which the parasitic side of gas-phase reactions is manifested in reduction of the growth efficiency depends on the MOCVD process conditions, reactor geometry features, and residence time of precursors; heat distribution profiles and temperature gradients. We have shown that device quality AlN-based heterostructures, and on a large 2 inch diameter size wafers, can successfully be achieved in a horizontal-type MOCVD reactor with merged jet of the precursors $(CH_3)_3Al$ and NH_3 – rather opposite to the common practice – provided optimization of the mixing point in a cool upstream region is achieved [38]. Other approaches to alleviate the parasitic side of gas-phase reactions involve the implementation of: (i) various modifications of the above referred flow-rate modulation epitaxy [11], which for a horizontal-type reactor introduces the precursors in a fashion that totally avoids their mixing, or (ii) vertical-type reactor designs with mixing of the precursors just shortly above the heated substrate [39].

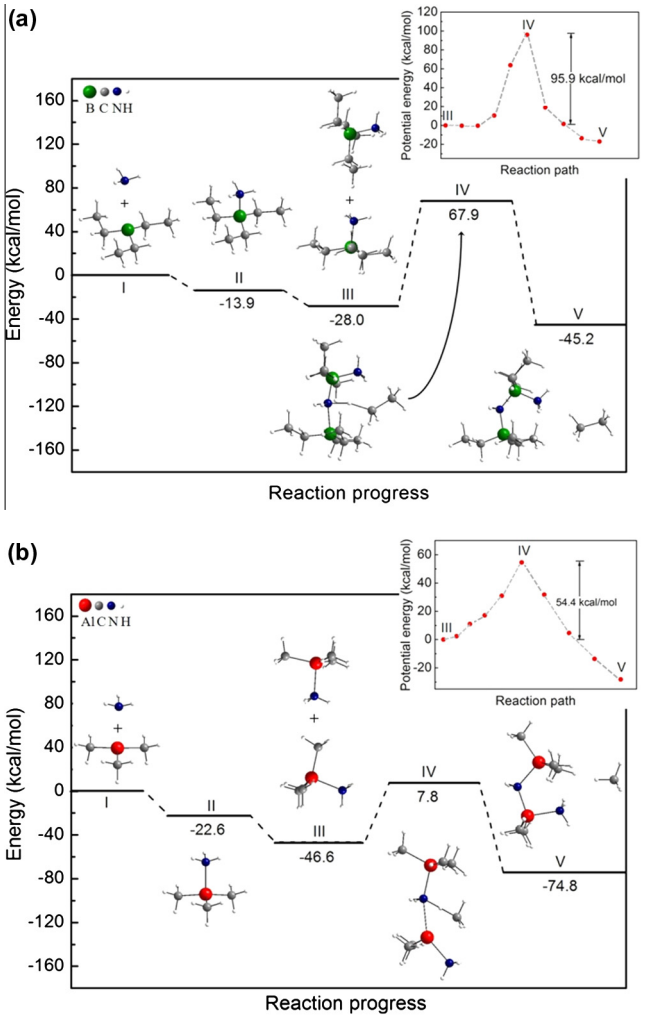

Figure 4. Schematic diagrams of sequences of gas-phase reactions starting with the formation of the (a) $(C_2H_5)_3B{:}NH_3$ adduct from the initial $(C_2H_5)_3B$ and NH_3 precursor molecules and further C_2H_6 elimination through the adduct-assisted reaction pathway (4); (b) $(CH_3)_3Al{:}NH_3$ adduct formation from the initial $(CH_3)_3Al$ and NH_3 precursor molecules and further CH_4 elimination through the adduct-assisted reaction pathway (7). The inset represents the minimum energy path between two equilibrium structures (III and V) of the overall gas-phase reaction. The line drawn to connect the points serves the only purpose of guiding the eye. The equilibrium structures of reaction species, corresponding to sequential steps I-to-V are depicted in each of the schematic diagrams.

The energy barrier to the RH (i.e., C_2H_6) elimination is raised through the transition state TS(3) in the presence of excess ammonia for the $(C_2H_5)_3B + NH_3$ system (Figure 3a). In a clear contrast, the energy barrier to the RH (i.e., CH_4) elimination is reduced through the transition state TS(6) in the presence of excess ammonia for the $(CH_3)_3Al + NH_3$ system (Figure 3b).

The coordination interaction of the $(CH_3)_3Al{:}NH_3$ adduct with a second ammonia molecule forms a stable transition state expressed by the gain of energy of ~1.0 kcal/mol. Formation of a stable transition state implies the possibility that the $(CH_3)_3Al{:}NH_3$ adduct could proceed to the generation of adduct-derived species in the gas-phase. While the ammonia-assisted reaction pathway can open an effective RH elimination channel in the $(CH_3)_3Al + NH_3$ system, the propagation of adduct-derived species in the gas-phase in the $(C_2H_5)_3B + NH_3$ system can be restrained.

The established difference in the reactivity of the $(C_2H_5)_3B{:}NH_3$ and $(CH_3)_3Al{:}NH_3$ adducts in the presence of excess ammonia might be accounted for the different coordination requirement of B and Al atoms. Yet, when same atoms are involved, difference in the reactivity is established due to steric repulsion between the ethyl groups and ammonia, which hardly takes place for the methyl groups [32]. Our results show that the second ammonia molecule comes to a shorter distance to the $(CH_3)_3Al{:}NH_3$ adduct. The respective Al–N bond length evolves from 1.67 Å, when the N–H bond in the second ammonia molecule is breaking, to 1.51 Å immediately after the methane molecule is eliminated. In the analogous coordination interaction, involving the $(C_2H_5)_3B{:}NH_3$ adduct, the respective B–N bond length evolves from 1.96 Å, when the N–H bond in the second ammonia molecule is breaking, to 1.83 Å immediately after the ethane molecule is eliminated.

With reference to the steric repulsion between the ethyl groups in two $(C_2H_5)_3B{:}NH_3$ adducts, which prohibits a strong coordination interaction, the energy barrier to the ethane elimination through the TS(4) in the adduct-assisted (4) reaction pathway is established to be further raised (Figure 4a) as compared with the ammonia-assisted (3), and particularly with the unimolecular (2), reaction pathways in the $(C_2H_5)_3B + NH_3$ system (Figures 2a and 3a, respectively). It is interesting to note that the replacement of one of the $(C_2H_5)_3B{:}NH_3$ adducts with a $(CH_3)_3Al{:}NH_3$ adduct can substantially reduce the energy barrier to the RH elimination (Figure 5) being manifestation of the impact of the strong Al–N coordination interaction.

Due to steric repulsion, though less pronounced between the smaller methyl groups in the $(CH_3)_3Al{:}NH_3$ adducts, the energy barrier to the methane elimination through the TS(7) in the adduct-assisted (7) reaction pathway, is raised (Figure 4b) as compared with the ammonia-assisted (6), and the unimolecular (5) reaction pathways in the $(CH_3)_3Al + NH_3$ system (Figures 2b and 3b, respectively). Nevertheless, the relative energies of the corresponding transition states for the RH (i.e., CH_4) elimination in the

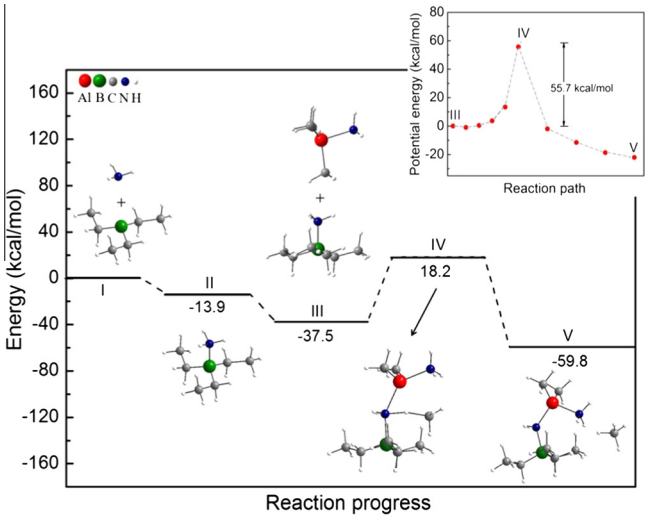

Figure 5. Schematic diagram of sequence of gas-phase reactions starting with the formation of the $(C_2H_5)_3B{:}NH_3$ adduct from the initial $(C_2H_5)_3B$ and NH_3 precursor molecules and further CH_4 elimination through an $(CH_3)_3Al{:}NH_3$ adduct-assisted reaction pathway. The inset represents the minimum energy path between two equilibrium structures (III and V) of the overall gas-phase reaction. The line drawn to connect the points serves the only purpose of guiding the eye. The equilibrium structures of reaction species, corresponding to sequential steps I-to-V are depicted in the schematic diagram.

$(CH_3)_3Al + NH_3$ system – TS(5) ~2.1 kcal/mol, TS(6) ~ – 1.0 kcal/mol, and TS(7) ~7.8 kcal/mol – are in the same order. The elimination of the RH (i.e., C_2H_6) in the $(C_2H_5)_3B + NH_3$ system is calculated to be energetically much more costly with relative energies of the corresponding transition states TS(2) ~22.2 kcal/mol, TS(3) ~45.9 kcal/mol, and TS(4) ~67.9 kcal/mol, of about an order of magnitude higher.

4. Conclusion

First-principles calculations, which also implement the NEB code, are performed to investigate the stability and subsequent reactivity of the $(C_2H_5)_3B{:}NH_3$ adduct formed by the initial precursor molecules $(C_2H_5)_3B$ and NH_3 in the MOCVD of hexagonal BN. Of the consistent gas-phase reaction pathways considered, ethane elimination from the adduct generating the amide monomer $(C_2H_5)_2BNH_2$ is characterized with the energy barrier of ~36 kcal/mol. As justified by the raise of the corresponding energy barriers, ~59 kcal/mol and 95 kcal/mol, ethane elimination is not facilitated by adduct reaction with neither a second ammonia molecule (NH_3 is in excess in the gas-phase) nor with a second adduct (the $(C_2H_5)_3B$ and NH_3 precursor molecules convert to adduct with no energy barrier). The $(C_2H_5)_3B{:}NH_3$ adduct appears stable against ethane elimination, suggestive that the propagation of adduct-derived species – capable to further react and complicate the overall gas-phase chemistry underlying the actual deposition mechanism – may essentially be precluded. A clear contrast can be noted with the reference case of the $(CH_3)_3Al{:}NH_3$adduct with facile methane elimination which is further promoted through the coordination interaction with a second NH_3 molecule. In terms of operating conventional MOCVD process, excess ammonia contributes active – and readily available – N-bearing species for deposition at the surface. The excess ammonia, however, promotes further the already high degree of reactivity of the $(CH_3)_3Al{:}NH_3$ adduct with known ultimate adverse effect on the growth efficiency in the deposition of AlN. It results from the propagation of less-volatile adduct-derived species in the gas-phase. The first-principles calculations in this study allow speculating that the excess ammonia in the deposition of BN operates to prevent any reactivity of the $(C_2H_5)_3B{:}NH_3$ adduct in the gas-phase.

Acknowledgements

Support by the Swedish Foundation for International Cooperation in Research and Higher Education (STINT), Project YR2009-7017, is gratefully acknowledged. G.K.G. and A.K.-G. acknowledge support by the Linköping Linnaeus Initiative on Novel Functionalized Materials (VR). A.K.-G. acknowledges support by the Swedish Governmental Agency for Innovation Systems (VINNOVA). R.R.Q.F., F.de B.M., and C.M.C. de C. acknowledge support by Conselho Nacional de Desenvolvimento Científico e Tecnológico (CNPq). R.R.Q.F. acknowledges specific support from Fundação CAPES. We thank Renato Batista dos Santos for the final formatting of the insets in the Figures 2–5.

References

[1] Y. Taniyasu, M. Kasu, T. Makimoto, Nature 441 (2006) 325.
[2] A. Khan, K. Balakrishnan, T. Katona, Nat. Photonics 2 (2008) 77.
[3] K. Watanabe, T. Taniguchi, H. Kanda, Nat. Mater. 3 (2004) 404.
[4] Y. Kobayashi, H. Hibino, T. Nakamura, T. Akasaka, T. Makimoto, N. Matsumoto, Jpn. J. Appl. Phys. 46 (2007) 2554.
[5] Y. Kobayashi, T. Akasaka, J. Cryst. Growth 310 (2008) 5044.
[6] Y. Kobayashi, C.-L. Tsai, T. Akasaka, Phys. Status Solidi C7 (2010) 1906.
[7] A.Y. Polyakov, M. Shin, W. Qian, M. Skowronski, D.W. Greve, R.G. Wilson, J. Appl. Phys. 81 (1997) 715.
[8] T. Takano, M. Kurimoto, J. Yamamoto, H. Kawanishi, J. Cryst. Growth 237 (2002) 972.
[9] R. Dahal, J. Li, S. Majety, B.N. Pantha, X.K. Cao, J.Y. Lin, H.X. Jiang, Appl. Phys. Lett. 98 (2011) 211110.
[10] S. Majety, J. Li, X.K. Cao, R. Dahal, B.N. Pantha, J.Y. Lin, H.X. Jiang, Appl. Phys. Lett. 100 (2012) 061121.
[11] T. Akasaka, T. Makimoto, Appl. Phys. Lett. 88 (2006) 041902.
[12] T. Akasaka, Y. Kobayashi, T. Makimoto, Appl. Phys. Lett. 91 (2007) 041914.
[13] A. Kakanakova-Georgieva, D. Nilsson, E. Janzén, J. Cryst. Growth 338 (2012) 52.
[14] H. Simka, B.G. Willis, I. Lengyel, K.F. Jensen, Prog. Cryst. Growth Charact. 35 (1977) 117.
[15] T.G. Mihopoulos, V. Gupta, K.F. Jensen, J. Cryst. Growth 195 (1998) 733.
[16] J.R. Creighton, W.G. Breiland, M.E. Coltrin, R.P. Pawlowski, Appl. Phys. Lett. 81 (2002) 2626.
[17] K. Matsumoto, A. Tachibana, J. Cryst. Growth 272 (2004) 360.
[18] J.R. Creighton, G. Wang, J. Phys. Chem. A109 (2005) 10554.
[19] A. Kakanakova-Georgieva, G.K. Gueorguiev, S. Stafström, L. Hultman, E. Janzén, Chem. Phys. Lett. 431 (2006) 346.
[20] A. Timoshkin, H.F. Schaefer III, J. Phys. Chem. C 112 (2008) 13816.
[21] J.P. Perdew, J.A. Chevary, S.H. Vosko, K.A. Jackson, M.R. Pederson, D.J. Singh, C. Fiolhais, Phys. Rev. B46 (1992) 6671.
[22] G. Kresse, J. Hafner, Phys. Rev. B47 (1994) 558.
[23] M.D. Wodrich, C. Corminboeuf, P. von RaguéSchleyer, Org. Lett. 8 (2006) 3631.
[24] G. Kresse, J. Hafner, Phys. Rev. B47 (1993) 558;
G. Kresse, J. Furthmüller, Phys. Rev. B54 (1996) 11169.
[25] G. Kresse, D. Joubert, Phys. Rev. B59 (1999) 1758.
[26] H. Jónsson, G. Mills, K.W. Jacobsen, Nudged elastic band method for finding minimum energy paths of transitions, in: B.J. Berne, G. Ciccotti, D.F. Coker (Eds.), Classical and Quantum Dynamics in Condensed Phase Simulations, World Scientific, Singapore, 1998, p. 385 (Chapter 16).
[27] G. Henkelman, H. Jónsson, J. Chem. Phys 113 (2000) 9978.
[28] D. Sheppard, R. Terrell, G. Henkelman, J. Chem. Phys. 128 (2008) 134106.
[29] G. Henkelman, B.P. Uberuaga, H. Jónsson, J. Chem. Phys 113 (2000) 9901.
[30] R.R. de Q. Freitas, R. Rivelino, F. de Brito Mota, C.M.C. de Castilho, J. Phys. Chem. C 116 (2012) 20306.
[31] B. Ómarsson, E.H. Bjarnason, S.A. Haughey, et al., Phys. Chem. Chem. Phys. 15 (2013) 4754.
[32] M. Ikenaga, K. Nakamura, A. Tachibana, K. Matsumoto, J. Cryst. Growth 237–239 (2002) 936.
[33] J.S. Lewis, S. Vaidyaraman, W.J. Lackey, P.K. Agrawal, G.B. Freeman, E.K. Barefield, Mater. Lett. 27 (1996) 327.
[34] K. Nakamura, J. Electrochem. Soc. 133 (1986) 1120.
[35] T.F. Kuech, E. Veuhoff, T.S. Kuan, V. Deline, R. Potemski, J. Cryst. Growth 77 (1986) 257.
[36] R.L. Moon, Y.-M. Houng, in: M.L. Hitchman, K.F. Jensen (Eds.), Chemical Vapor Deposition, Academic Press Ltd., 1993 (ISBN 0-12-349670-5, Chapter 6).
[37] D. Sengupta, J. Phys. Chem. B107 (2003) 291.
[38] A. Kakanakova-Georgieva, R.R. Ciechonski, U. Forsberg, A. Lundskog, E. Janzén, Cryst. Growth Des. 9 (2009) 880.
[39] M. Dauelsberg, E.J. Thrush, B. Schineller, J. Kaeppeler, in: M. Razeghi, M. Henini (Eds.), Optoelectronic Devices: III-Nitrides, Elsevier Ltd., 2004 (ISBN: 0-08-044426-1, Chapter 4).